Low-Frequency Variability and the Unusual Indian Ocean Dipole Events in 2015 and 2016

Lianyi Zhang[1,2] [iD], **Yan Du[1,2]** [iD], and **Wenju Cai[3,4]** [iD]

[1]State Key Laboratory of Tropical Oceanography, SCSIO, CAS, Guangzhou, China, [2]College of Earth Science, University of Chinese Academy of Sciences, Beijing, China, [3]CSIRO Marine and Atmospheric Research, Aspendale, Victoria, Australia, [4]Physical Oceanography Laboratory/CIMSST, Ocean University of China and Qingdao National Laboratory for Marine Science and Technology, Qingdao, China

Abstract An unusual positive Indian Ocean Dipole (IOD) event occurred in 2015 associated with the 2015/2016 extreme El Niño. Unlike the canonical IOD, sea surface temperature (SST) warming in the west central tropical Indian Ocean (TIO) dominated the strong zonal SST gradient as cooling off Sumatra-Java was weak. Over the southeastern TIO, deeper thermocline has suppressed the upwelling cooling since 2012. Such deepened thermocline related to a low-frequency adjustment and curtailed cool anomalies in the 2015 positive IOD but favored warm anomalies in the 2016 negative IOD. Based on statistical analyses, ocean assimilation data confirm that an IOD-like pattern exists in the TIO on decadal timescale. During a negative decadal IOD-like phase, thermocline is deeper in the southeastern TIO; the thermocline-SST feedback is unfavorable for positive IOD occurrence and intensity, but conducive to negative IOD events. Thus, we propose that the 2015–2016 IOD events are modulated by the low-frequency variability of thermocline.

1. Introduction

The Indian Ocean Dipole (IOD) is an intrinsic climate mode in the tropical Indian Ocean (IO). A positive IOD (pIOD) event is characterized by sea surface temperature (SST) cooling in the southeastern tropical IO (SETIO) as the eastern pole, and warming in the western tropical IO (WTIO) as the western pole (Saji et al., 1999; Webster et al., 1999). Normally, an IOD event tends to develop in boreal summer (June–August, JJA) and mature in fall (September–November, SON), showing significant seasonality (Saji et al., 1999; Yang et al., 2015). During a pIOD event, equatorial easterly wind enhances coastal upwelling off Sumatra/Java, resulting in SST cooling in the eastern pole, whereas in the western pole, SST warming enhances the local deep convection and rainfall, shifting the upward branch of the Walker Circulation westward (Ashok et al., 2001; Li et al., 2003; Schott & McCreary, 2001).

The eastern pole of the IOD, which is usually regarded as the dominant pole, has larger SST variability amplitude due to active thermocline-SST feedback (Behera & Yamagata, 2003; Webster et al., 1999). The thermocline-SST feedback, thermocline shoaling leading to SST cooling, plays a major role in the IOD development and evolution (Annamalai et al., 2003; Cai et al., 2013). During a pIOD event, coastal upwelling induced by easterly wind anomalies generates SST cooling off Sumatra/Java. The enhanced west-minus-east zonal SST gradient, in turn, intensifies the wind anomalies (Li et al., 2003; Saji et al., 1999), triggering a Bjerknes feedback in the tropical IO (Bjerknes, 1969; Li et al., 2003; Meyers et al., 2007; Webster et al., 1999).

As the strongest interannual climate mode in the tropics, the El Niño/Southern Oscillation (ENSO) exerts an influence on the IOD (Allan et al., 2001; Annamalai, Xie, et al., 2005; Ashok et al., 2003; Behera et al., 2006; Luo et al., 2010). During the developing phase of the El Niño, the slowdown of the Walker Circulation results in surface easterly wind anomalies in the equatorial IO, triggering a pIOD event (Behera et al., 2006; Yuan et al., 2013). For example, the strong 1997 pIOD co-occurred with a strong El Niño (Table S1 and Figure S1 in the supporting information) (Murtugudde et al., 2000; Trenberth, 1997; Yu & Rienecker, 1999), while the 2015 pIOD was rather different. Even though concurrent with an extreme El Niño, the 2015 pIOD was a moderate event, and SST cooling in the SETIO was weak (Table S1 and Figure 1). The western pole rather than the eastern pole played a dominant role.

However, a pIOD (nIOD) can be independent from an El Niño (La Niña). For example, among the three consecutive pIOD events during 2006–2008, the 2007 and 2008 events were accompanied by a weak La Niña (Cai et al., 2009; Luo et al., 2008; Rao et al., 2008). Moreover, although the tropical Pacific is in a neutral state, a
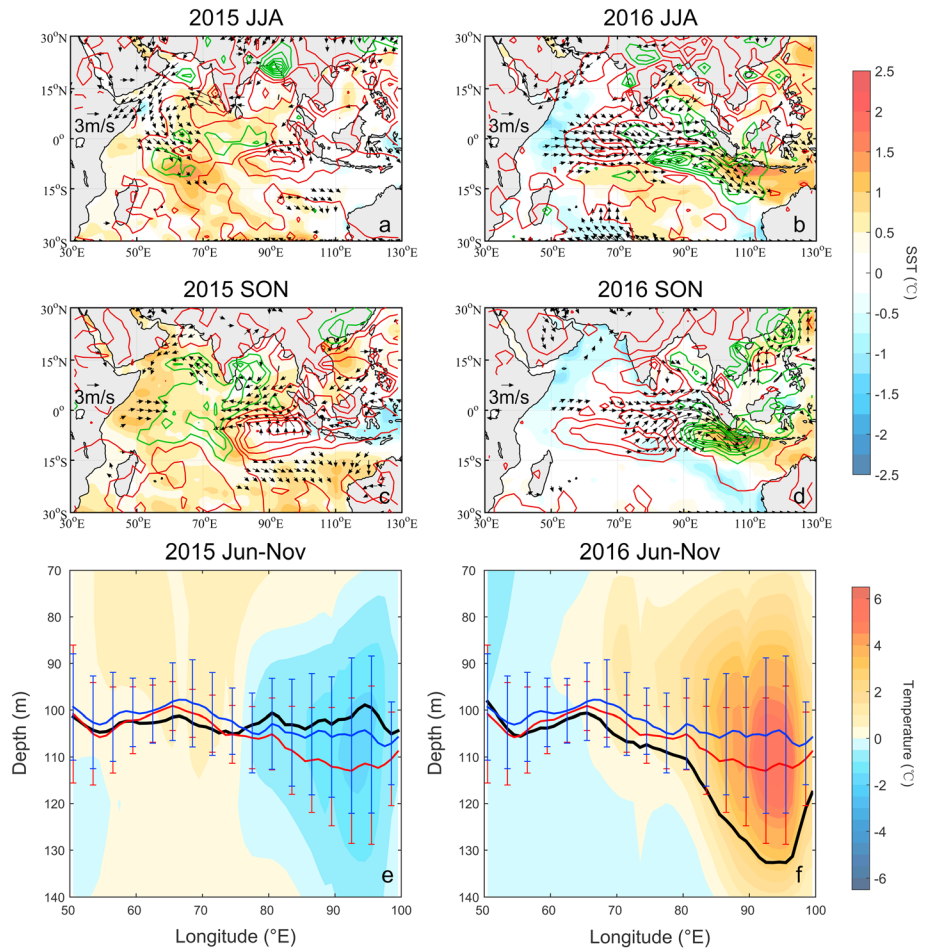
Figure 1. IOD events in 2015–2016. Trimonthly mean of anomalous sea surface temperature (OISST, shading, °C), precipitation (CMAP, contour, interval by 1.5 mm d^{-1}, green for wetter and red for drier), and wind (NCEP, vector, m s^{-1}) for the pIOD events during the developing (June–August, JJA) and peak (September–November, SON) phase in (a, c) 2015 and (b, d) 2016, respectively. We omit the wind vectors with amplitude of wind anomaly lower than 1.5 m/s. June–November mean of vertical temperature (shading, °C) and 22°C isothermal depth (D22, black lines, meter) based on Argo along the equator in the Indian Ocean (2°E–2°S) in (e) 2015 and (f) 2016. The blue and red lines indicate the averaged D22 in June–November of 2006–2010 and 2012–2016, respectively. The error bar stands for standard deviation of D22 in corresponding period.

negative IOD (nIOD), one of the strongest nIOD events on record, occurred in 2016. The dynamic behind these unusual features were not clear.

Similar to the ENSO featuring decadal variations (Yeh, 2005), the IOD is associated with longer timescale variability (Han et al., 2014). The IOD shows varying characteristics due to variability in the Walker Circulation, the IO monsoon, and the subtropical high (Ashok et al., 2004; Shi et al., 2007; Tozuka et al., 2007; Yeh, 2005; Yuan et al., 2008). Ummenhofer et al. (2017) pointed out that the stronger IOD events in 1990s are a result of the Indo-Pacific decadal variability. Here we propose a hypothesis that the low-frequency variability contributes to the unusual characteristics of the IOD events in 2015 and 2016 and further investigate the thermocline-SST feedback in different decadal phases.

2. Data and Methods

We use Optimum Interpolation Sea Surface Temperature (OISST) data provided by National Oceanic and Atmospheric Administration (NOAA) to illustrate the IOD events since 1982 (Reynolds et al., 2002). A dipole mode index (DMI) is defined as the difference of area-mean SST between the western pole (WTIO,

50°E–70°E, 10°S–10°N) and the eastern pole (SETIO, 90°E–110°E, 10°S–0°) (Saji et al., 1999). Also used are sea level pressure (SLP) and surface winds available in 1948–2017 from the National Centers for Environmental Prediction-National Center for Atmospheric Research (NCEP-NCAR) reanalysis data (Kalnay et al., 1996). The precipitation from the Climate Prediction Center Merged Analysis of Precipitation (CMAP) are in the period of 1979–2017 (Xie & Arkin, 1997). The ocean temperature data are from NCEP Global Ocean Data Assimilation System (GODAS) during 1980 to present (Saha et al., 2006) and Gridded Argo database created by Scripps Institution of Oceanography since 2004 (Holte et al., 2017). Simple Ocean Data Assimilation (SODA, version 2.2.4) product, an ocean assimilation data set covering the global ocean in the period of 1871–2010 with a resolution of 0.5° × 0.5°, is used to examine low-frequency variability in the IO (Carton & Giese, 2008). Furthermore, the Extended Reconstructed SST V3b (ERSST) is used to analyze the low-frequency SST variability in a long-term context covering a period of 1871 to present (Smith et al., 2008).

The anomalies are obtained by subtracting the monthly climatology from the original data. All linear trends are removed except for Figure 1 that presents the primary IOD events. In this study, we use the Butterworth low-pass filter with an order of 6 and cutoff frequency of 5 years to obtain the low-frequency variability. Due to limitation of the low-pass filter, the endpoint values with length of 2.5 years are omitted in the figures.

3. Results

### 3.1. The 2015–2016 IOD Events

A moderate pIOD event occurred in 2015 without a significant SST cooling in the SETIO (Figures 1a, 1c, and 1e). Rather, a strong SST warming occurred in the WTIO. The SST warming appeared in the central and southern tropical IO along with cyclonic wind anomalies during boreal summer. The anomalous winds opposed the summer monsoon and hence reduced surface evaporation in the WTIO. As a result, surface water warmed rapidly in the following fall season (Figures 1a and 1c). In the fall, weak easterly wind anomalies caused slight upwelling and SST cooling in the SETIO (Figures 1c and 1e). The eastern pole had little contribution to the 2015 pIOD.

By contrast, a nIOD event, one of the strongest events on record, occurred in following year (Figures 1b, 1d, and 1f), while the tropical Pacific featured a weak cooling or a neutral condition, differing from the 1998 nIOD event that was accompanied by a strong La Niña (Table S1 and Figure S1). In JJA of 2016, westerly wind anomalies prevailed along the equatorial IO, resulting in a strong east-west thermocline tilt (deeper in the east, Figure 1f). The deep thermocline favored SST warming in the SETIO and led to excessive rainfall over the region. In SON, the significant SST warming in the SETIO facilitated the Bjerknes feedback, leading to the strong nIOD event.

The eastern pole plays a rather different role during the sequence of events. Given the potential influence of the mean state, the changes of thermocline depth could significantly influence the thermocline-SST feedback (Cai et al., 2013). We examine the thermocline depth difference during the 2006–2010 and the 2012–2016 periods with a 5 year time window. The thermocline is deeper in the eastern equatorial IO in boreal summer-autumn during the latter period (Figures 1e and 1f), unfavorable to SST cooling off Suma-Java and hence the 2015 pIOD. Even in the first half year of these two periods, the deepened thermocline could be observed (Figure S2). Due to the deepened thermocline, the upwelling is weakened, associated with a weak thermocline-SST feedback, hence a weak SST cooling. On the other hand, the deepened thermocline sustains SST warming by enhancing downwelling process. Thus, it is important to understand the difference of thermocline between different periods.

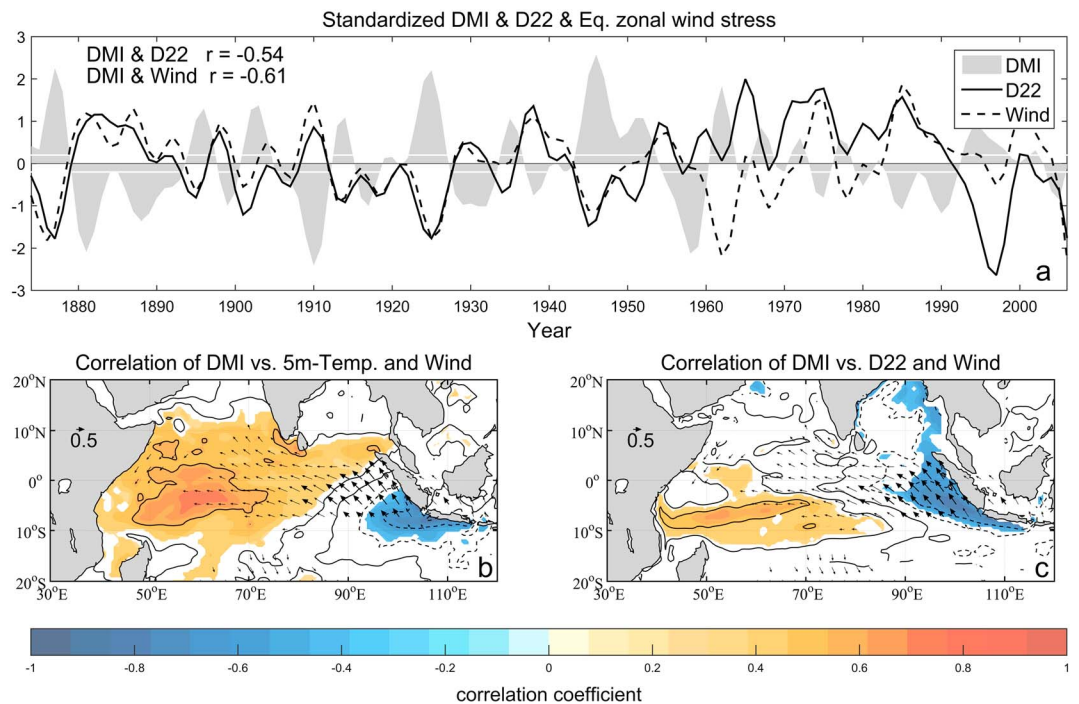### 3.2. Low-Frequency Variability

Previous studies suggested that low-frequency variability might explain changes of the mean thermocline depth on decadal timescale in the eastern equatorial IO (Annamalai, Potemra, et al., 2005; Krishnamurthy & Krishnamurthy, 2015; Ummenhofer et al., 2017). The low-frequency variations in the Pacific, such as the Pacific Decadal Oscillation (PDO), could induce changes in the tropical atmospheric circulation, thus influence the IO (e.g., Annamalai, Potemra, et al., 2005). In addition, an oceanic pathway in the Indonesia Seas was suggested to convey such signals (e.g., Schwarzkopf & Böning, 2011). Figure 2 displays the low-frequency variabilities of SST, SSH, SLP, and surface wind in the equatorial IO. The coupled ocean-atmosphere interactions show variations on decadal timescales. For example, after 2012, the low-frequency DMI (black curve,
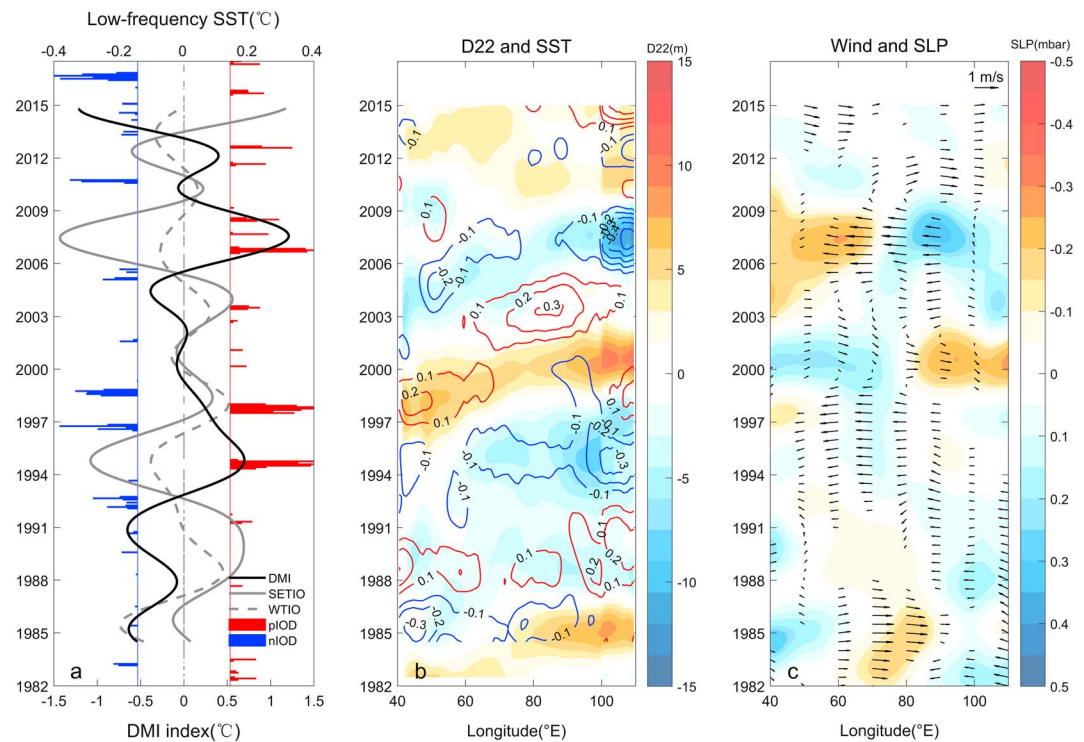
Figure 2. Low-frequency variations along equatorial IO since 1982. (a) Time series of 5 year low-pass-filtered DMI (black line), SST in the WTIO (gray dashed line), and SETIO (gray line) based on OISST. Red and blue bars indicate positive/negative IOD (pIOD/nIOD) when the DMI is greater/smaller than 1/−1 standard deviation (0.47°C). (b) Low-frequency variability of D22 (GODAS, shading, meter) and SST (OISST, contour, interval by 0.1°C, red for warmer, blue for cooler) in the equatorial IO (meridional-mean of 2°S–2°N in 40°E–100°E) and the nearshore area along Sumatra/Java coast (from 100°E, 0° to 110°E, 10°S). (c) Same as Figure 2b but for SLP (shading, mbar) and surface wind (vector, m/s) from NCEP averaged over 5°S–5°N along the equator from 40°E to 110°E. The SLP is shown as the zonal departure field due to the gradient force on wind, which is calculated as the local SLP anomaly subtracting the concurrent area-mean SLP anomaly along the equator. We omit the wind with amplitude of wind anomaly lower than 0.2 m/s. All linear trends are removed. The low-frequency endpoint values with length of 2.5 years are omitted in this analysis.

Figure 2a) tends to be negative, corresponding to deeper thermocline, SST warming in SETIO (Figure 2b), and westerly wind anomalies along the equator (Figure 2c). In 2012–2016, although the recent 2.5 year result was omitted due to the limitation of low-pass filter processing, a nIOD-like low-frequency state with a warmer eastern pole and equatorial westerly wind anomalies were seen for the prior years. It was consistent with the thermocline shown in Figure 1, providing a precondition for the 2015–2016 events (Figures 2b and 2c).

Low-frequency variability also plays an important role in other periods (Figure 2). For instance, the strong 1994 pIOD event did not occur with an El Niño but developed with a contribution from the favorable low-frequency variability. A cooler eastern pole was sustained by a shallower thermocline and easterly winds in low frequency since 1990, which persisted to early 1999, and potentially influenced the 1997 pIOD. Another example is the three consecutive positive IOD events in 2006–2008 (Cai et al., 2009). After a warm phase in the period of 2000–2005, the shallow thermocline in the eastern pole again favored easterly winds along the equator and the SST cooling off Sumatra/Java, despite the fact the Pacific features a weak La Niña in 2008 (Table S1). To assess longer timescale variability by other mathematical method, we also use an Empirical Mode Decomposition (EMD) (Huang et al., 1998; Torres et al., 2011) to separate monthly DMI in different timescale (Figures S3a–S3c). The contribution from the low-frequency variability (22%) is considerable, which is more than a half of the interannual variability (43%). A harmonic analysis on monthly DMI shows low-frequency spectrum peaks at 5 years, 10 years, and 24 years (Figure S3d). The long-term result based on ERSST and SODA since 1871 also suggest the coupled oscillation (Figure S4). Therefore, low-frequency variability appears to be modulating the IOD activities.
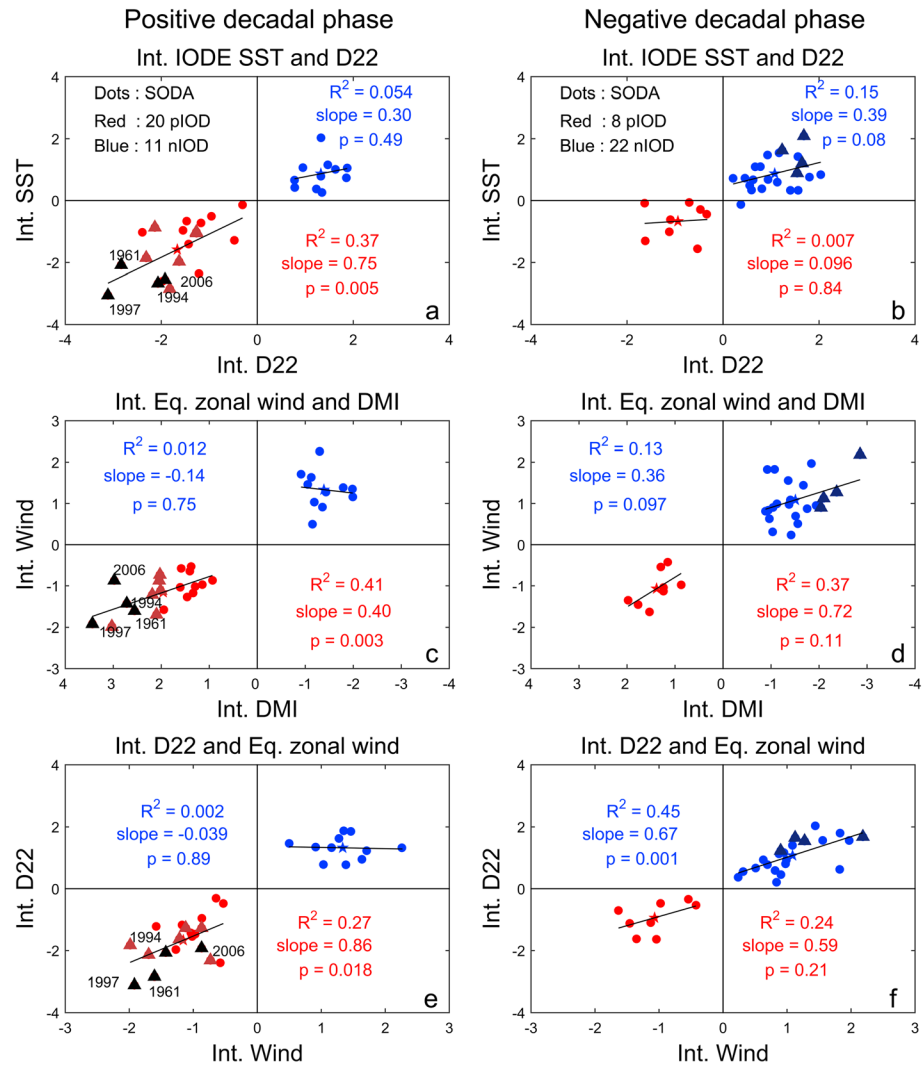
Figure 3. Features of low-frequency variability. (a) Standardized low-frequency indices of DMI (shading), D22 in the SETIO (black line), and zonal wind stress along the equator (dashed line) based on SODA data. Equatorial zonal wind stress is averaged over equatorial IO (70°E–90°E, 5°N–5°S). The low-frequency indices refers to the 5 year low-pass-filtered results. The *r* stands for correlation coefficient (both $p < 0.01$). The decadal IOD phase is defined by when low-frequency DMI is greater/smaller than 0.2/−0.2 standard deviation (indicated by white line). Correlation of the low-frequency DMI with (b) temperature at 5 m layer (contour, intervals of 0.1) and wind stress (vector) and (c) the D22 (contour) and wind stress (vector) in the tropical IO. The shading and bold arrows in Figures 3b and 3c pass 95% confidence level by two-tailed Student's *t* test. The linear trends are removed from the original data. All the results are normalized and based on SODA in the period of 1871–2010.

3.3. Thermocline-SST Feedback

The thermocline-SST feedback is the key to understanding the decadal modulation on the IOD. Based on SODA, a thermocline index (D22) is defined as the area-averaged depth of 22°C isothermal over the SETIO. The area average of zonal wind stress anomalies over the equatorial region (70°E–90°E, 5°N–5°S) is used as a wind index to represent the atmospheric response. To construct low-frequency indices, a 5 year low-pass filter and a normalization procedure are applied to the D22, the wind index, and the DMI. The D22 and wind index vary with the DMI, with correlation coefficients about −0.54 and −0.61, respectively (both of *p* values smaller than 0.01; Figure 3a), suggesting an ocean-atmosphere coupling at low frequency. The correlation of D22, SST, and wind stress fields with the low-frequency DMI exhibits a pIOD-like feature, hereafter referred to as decadal IOD (Figures 3b and 3c) (Tozuka et al., 2007). We define a positive (negative) decadal IOD phase as when the low-frequency DMI is greater (smaller) than 0.2 standard deviation (Figure 3a). A positive decadal phase indicates a shallower thermocline and SST cooling in the SETIO, southeasterly wind anomalies over the equatorial region, and vice versa (Figures 3b and 3c).

The relationships among D22, SST, and zonal wind reflect the efficiency of the thermocline-SST-wind feedback. Hence, we investigate the activity of the interannual IOD during positive/negative decadal IOD phases by subtracting the 5 year low-pass-filtered results from the original signal. Only significant events are considered (see standard in the caption of Figure 4). Consequently, 20 (8) and 11 (22) interannual pIOD and nIOD are identified during the positive (negative) decadal IOD phase, respectively (Figure 4). Here we mainly show the statistical results without low-frequency variability; the results for all events and results retaining low-frequency variability are shown in the supporting information figures (Figures S5 and S6). The small change of the number of total IOD events after removing low-frequency variability does not affect our analyses (Figure S5).

Figure 4. Scatter diagrams for IOD activity in different decadal IOD phases. The interannual (Int.) variability is obtained by removing low-frequency variability from original data. Int. IOD eastern pole (IODE) SST versus Int. D22 in the (a) positive and (b) negative decadal phase. Similarly, (c, d) for DMI versus equatorial (Eq.) zonal wind and (e, f) for D22 versus Eq. zonal wind. The significant events are selected based on the standard that DMI is greater/smaller than $0.8/-0.8$ standard deviation along with equatorial easterly/westerly wind anomalies and thermocline shoaling/deepening in the SETIO. The months that meet the standard in the June–December of IOD year are averaged. The stars refer to mean intensity. The extreme pIOD/nIOD events in dark red/blue triangles and four typical pIOD events (1961, 1994, 1997, and 2006) are in black color. The regression parameters including R^2, slope, and p value are shown in the figures. The linear trends are removed from the original data. All the results are normalized and based on SODA in the period of 1871–2010.

The interannual pIOD (nIOD) occurs more frequently in the positive (negative) decadal phase no matter whether the low-frequency variability exists (Figures 4 and S6); however, such asymmetry decrease slightly after removing the low-frequency variability. During the positive decadal phase, the SETIO thermocline is shallower, enhancing the thermocline-SST feedback and consequently favoring more pIOD events. Similar result can be found in the wind versus SST and wind versus thermocline (red dots, Figures 4a, 4c, and 4e), implying stronger coupled ocean-atmosphere processes for pIOD events. Besides, the strong positive (negative) IOD events tend to appear in the corresponding positive (negative) decadal period. For example, the extreme pIOD events, interannual DMI greater than a 2 standard deviation value, only appear in the positive decadal phase, such as in 1994, 1997, and 2006 (dark red and black triangles, Figures 4a, 4c, and 4e).

During the negative decadal phase, as that for the 2015 pIOD and 2016 nIOD, the thermocline-SST feedback is not as effective as that during the positive decadal phase. The deeper thermocline makes the thermocline-

SST coupling ineffective particularly for the pIOD (Figure 4b). For the pIOD, although equatorial zonal winds still respond to SST gradient (red dots, Figure 4d), the response of thermocline to equatorial winds is NOT as effective (red dots, Figure 4f), when compared with pIOD events during the positive decadal phase (red dots, Figure 4e), consistent with what is expected from a deeper thermocline. For the nIOD, the coupling seems still strong, but the eastern pole moves a little bit to east, choked along the upwelling region off Java (e.g., 2016 nIOD in Figure 1d). The big enhancement, when compared to the nIOD in the positive decadal phase, is the relationship of equatorial zonal westerly wind with SST gradient and thermocline (compare blue dots of Figures 4c versus 4d and Figures 4e versus 4f). This suggests that westerly wind plays an important role in promoting the development of nIOD during negative decadal phase. The SST gradient enhances the westerly wind (Figure 4d); the wind further forces the warmer water accumulated along the Sumatra/Java coastline and deepening the thermocline (Figure 4f). In summary, since 2012, the mean state has been in a negative decadal phase in the equatorial IO. Based on the statistical results, we propose that this mean state has the effect of sustaining warm anomalies as in 2016 but undermining cool anomalies in the eastern equatorial IO in 2015.

4. Conclusion and Discussion

In this study, using available observational data, we report an unusual moderate pIOD event that occurred in 2015, concurrent with an extreme El Niño event. The pIOD event featured a strong SST warming in the west central IO and weak SST cooling in the SETIO (Figures 1a, 1c, and 1e). Following this unconventional pIOD, the strongest nIOD event on record occurred in 2016 (Figures 1b, 1d, and 1f). We also find significant decadal IOD-like variations in the tropical IO (Figures 2 and 3), a low-frequency coupled ocean-atmosphere oscillation affecting interannual IOD events through varying strength of the thermocline-SST-wind feedback (Figure 4). As the statistical analyses suggest, the unusual pIOD and strong nIOD could be the consequence of such low-frequency variability.

The ocean mean state in the eastern equatorial IO exhibited a deeper thermocline in 2012–2016 (Figures 1e and 1f) than in 2006–2010. The thermocline-SST feedback in the eastern IO is different between the two decadal phases, constituting a modulation of decadal variability on interannual IOD properties (Figure 4). During the positive decadal phase as in 2006–2010, a shallower-than-normal thermocline in the SETIO is more effective in generating cold SST anomalies. As such, the frequency and intensity of pIOD events are significantly enhanced (Figures 4a, 4c, and 4e). During the negative decadal phase as in 2012–2016, due to deeper-than-normal thermocline in the SETIO, upwelling becomes weak and unfavorable to SST cooling but less unfavorable to SST warming. The thermocline-SST-wind feedback of the nIOD, however, is enhanced. The response of equatorial winds to zonal SST gradient remains rather effective, leading to a deeper thermocline and further development of warm SST anomalies in the SETIO (Figures 4b, 4d, and 4f). As such, the frequency and intensity of IOD events are significantly affected by the mean state.

Despite of different decadal phases, there is an IOD asymmetry caused by deeper mean thermocline in the SETIO, a positive skewness that the amplitude of pIOD tends to be stronger than nIOD (Cai et al., 2013). Oceanic advection could also contribute to the IOD asymmetry. Ocean currents induced by the easterly wind anomalies tend to generate a stronger advection of cooler water westward from the Sumatra/Java coast to the equatorial IO in a pIOD than that in a nIOD, expanding the SST cooling hence enhancing the Bjerknes feedback (Figures 1d and S1c).

There are different views on the generation of decadal variability in the IO such as the decadal IOD-like structure. One view is that it could be attributed to an asymmetric in the IOD occurrence and intensity, or to a remote external forcing, for example, the PDO from the Pacific (e.g., Tozuka et al., 2007; Ummenhofer et al., 2017). Tozuka et al. (2007) attributed the decadal IOD to a varying frequency of interannual IOD events, associated with variability in southward Ekman heat transport and the Mascarene High activities. On the other hand, via an oceanic pathway including the Indonesian Archipelago, low-frequency signals, like the PDO or Interdecadal Pacific Oscillation (IPO), were suggested to transmit from the Pacific to the IO (Annamalai, Potemra, et al., 2005; Schwarzkopf & Böning, 2011; Shi et al., 2007; Yang et al., 2017), which could affect the mean state of the tropical IO and interannual variability (Dong et al., 2016; Dong & McPhaden, 2017). Regardless of the different origins of the decadal variability, this study proposes that the low-frequency variability could modulate the interannual IOD events and contribute to the unusual 2015 pIOD and 2016 nIOD.

To further understand the interannual behavior in the different decadal phase and the way in which the modulation works, it is necessary to use a coupled ocean-atmosphere model to test the impact of decadal IOD mean state. Other issues to focus include the respective role of the two poles of decadal IOD, which are located in the thermocline dome in the southwest tropical IO and Sumatra/Java coast in the SETIO, respectively (Figure 3b). Both poles are south of equator, raising the possibility of a contribution from the Southern Hemisphere middle latitude, as suggested by Tozuka et al. (2007). Investigation of the impact from midlatitude of Southern Hemisphere await further studies.

References

Allan, R. J., Chambers, D., Drosdowsky, W., Hendon, H., Latif, M., Nicholls, N., … Tourre, Y. (2001). Is there an Indian Ocean Dipole, and is it independent of the El Niño–Southern Oscillation? *Clivar Exchanges*, 6(3), 18–22.

Annamalai, H., Murtugudde, R., Potemra, J., Xie, S. P., Liu, P., & Wang, B. (2003). Coupled dynamics over the Indian Ocean: Spring initiation of the zonal mode. *Deep Sea Research Part II: Topical Studies in Oceanography*, 50(12-13), 2305–2330. https://doi.org/10.1016/s0967-0645(03)00058-4

Annamalai, H., Potemra, J., Murtugudde, R., & McCreary, J. P. (2005). Effect of preconditioning on the extreme climate events in the tropical Indian Ocean. *Journal of Climate*, 18(17), 3450–3469. https://doi.org/10.1175/Jcli3494.1

Annamalai, H., Xie, S. P., McCreary, J. P., & Murtugudde, R. (2005). Impact of Indian Ocean sea surface temperature on developing El Nino. *Journal of Climate*, 18(2), 302–319. https://doi.org/10.1175/Jcli-3268.1

Ashok, K., Chan, W.-L., Motoi, T., & Yamagata, T. (2004). Decadal variability of the Indian Ocean Dipole. *Geophysical Research Letters*, 31, L24207. https://doi.org/10.1029/2004GL021345

Ashok, Z., Guan, Y., & Yamagata, T. (2001). Impact of the Indian Ocean Dipole on the relationship between the Indian monsoon rainfall and ENSO. *Geophysical Research Letters*, 28(23), 4499–4502. https://doi.org/10.1029/2001GL013294

Ashok, Z., Guan, Y., & Yamagata, T. (2003). A look at the relationship between the ENSO and the Indian Ocean Dipole. *Journal of the Meteorological Society of Japan*, 81(1), 41–56. https://doi.org/10.2151/Jmsj.81.41

Behera, S. K., Luo, J. J., Masson, S., Rao, S. A., Sakum, H., & Yamagata, T. (2006). A CGCM study on the interaction between IOD and ENSO. *Journal of Climate*, 19(9), 1688–1705. https://doi.org/10.1175/Jcli3797.1

Behera, S. K., & Yamagata, T. (2003). Influence of the Indian Ocean Dipole on the southern oscillation. *Journal of the Meteorological Society of Japan*, 81(1), 169–177. https://doi.org/10.2151/Jmsj.81.169

Bjerknes, J. (1969). Atmospheric teleconnections from the equatorial Pacific. *Monthly Weather Review*, 97(3), 163–172. https://doi.org/10.1175/1520-0493(1969)097%3C0163:atftep%3E2.3.co;2

Cai, W., Pan, A., Roemmich, D., Cowan, T., & Guo, X. (2009). Argo profiles a rare occurrence of three consecutive positive Indian Ocean Dipole events, 2006–2008. *Geophysical Research Letters*, 36, L08701. https://doi.org/10.1029/2008GL037038

Cai, W., Zheng, X.-T., Weller, E., Collins, M., Cowan, T., Lengaigne, M., … Yamagata, T. (2013). Projected response of the Indian Ocean Dipole to greenhouse warming. *Nature Geoscience*, 6(12), 999–1007. https://doi.org/10.1038/ngeo2009

Carton, J. A., & Giese, B. S. (2008). A reanalysis of ocean climate using Simple Ocean Data Assimilation (SODA). *Monthly Weather Review*, 136(8), 2999–3017. https://doi.org/10.1175/2007mwr1978.1

Dong, L., & McPhaden, M. J. (2017). Why has the relationship between Indian and Pacific Ocean decadal variability changed in recent decades? *Journal of Climate*, 30(6), 1971–1983. https://doi.org/10.1175/jcli-d-16-0313.1

Dong, L., Zhou, T., Dai, A., Song, F., Wu, B., & Chen, X. (2016). The footprint of the Inter-decadal Pacific Oscillation in Indian Ocean sea surface temperatures. *Scientific Reports*, 6(1), 21,251. https://doi.org/10.1038/srep21251

Han, W. Q., Vialard, J., McPhaden, M. J., Lee, T., Masumoto, Y., Feng, M., & de Ruijter, W. P. M. (2014). Indian Ocean decadal variability: A review. *Bulletin of the American Meteorological Society*, 95(11), 1679–1703. https://doi.org/10.1175/bams-d-13-00028.1

Holte, J., Talley, L. D., Gilson, J., & Roemmich, D. (2017). An Argo mixed layer climatology and database. *Geophysical Research Letters*, 44, 5618–5626. https://doi.org/10.1002/2017GL073426

Huang, N. E., Shen, Z., Long, S. R., Wu, M. L. C., Shih, H. H., Zheng, Q. N., … Liu, H. H. (1998). The empirical mode decomposition and the Hilbert spectrum for nonlinear and non-stationary time series analysis. *Proceedings of the Royal Society A: Mathematical, Physical & Engineering Science*, 454(1971), 903–995. https://doi.org/10.1098/rspa.1998.0193

Kalnay, E., Kanamitsu, M., Kistler, R., Collins, W., Deaven, D., Gandin, L., … Joseph, D. (1996). The NCEP/NCAR 40-year reanalysis project. *Bulletin of the American Meteorological Society*, 77(3), 437–471. https://doi.org/10.1175/1520-0477(1996)077%3C0437:Tnyrp%3E2.0.Co;2

Krishnamurthy, L., & Krishnamurthy, V. (2015). Decadal and interannual variability of the Indian Ocean SST. *Climate Dynamics*, 46(1-2), 57–70. https://doi.org/10.1007/s00382-015-2568-3

Li, T., Wang, B., Chang, C. P., & Zhang, Y. S. (2003). A theory for the Indian Ocean Dipole-zonal mode. *Journal of the Atmospheric Sciences*, 60(17), 2119–2135. https://doi.org/10.1175/1520-0469(2003)060%3C2119:Atftio%3E2.0.Co;2

Luo, J. J., Behera, S. K., Masumoto, Y., Sakuma, H., & Yamagata, T. (2008). Successful prediction of the consecutive IOD in 2006 and 2007. *Geophysical Research Letters*, 35, L14S02. https://doi.org/10.1029/2007GL032793

Luo, J. J., Zhang, R. C., Behera, S. K., Masumoto, Y., Jin, F. F., Lukas, R., & Yamagata, T. (2010). Interaction between El Niño and extreme Indian Ocean Dipole. *Journal of Climate*, 23(3), 726–742. https://doi.org/10.1175/2009jcli3104.1

Meyers, G., McIntosh, P., Pigot, L., & Pook, M. (2007). The years of El Niño, La Niña, and interactions with the tropical Indian Ocean. *Journal of Climate*, 20(13), 2872–2880. https://doi.org/10.1175/jcli4152.1

Murtugudde, R., McCreary, J. P., & Busalacchi, A. J. (2000). Oceanic processes associated with anomalous events in the Indian Ocean with relevance to 1997–1998. *Journal of Geophysical Research*, 105(C2), 3295–3306. https://doi.org/10.1029/1999JC900294

Rao, S. A., Luo, J.-J., Behera, S. K., & Yamagata, T. (2008). Generation and termination of Indian Ocean Dipole events in 2003, 2006 and 2007. *Climate Dynamics*, 33(6), 751–767. https://doi.org/10.1007/s00382-008-0498-z

Reynolds, R. W., Rayner, N. A., Smith, T. M., Stokes, D. C., & Wang, W. Q. (2002). An improved in situ and satellite SST analysis for climate. *Journal of Climate*, 15(13), 1609–1625. https://doi.org/10.1175/1520-0442(2002)015%3C1609:Aiisas%3E2.0.Co;2

Saha, S., Nadiga, S., Thiaw, C., Wang, J., Wang, W., Zhang, Q., … Xie, P. (2006). The NCEP climate forecast system. *Journal of Climate*, 19(15), 3483–3517. https://doi.org/10.1175/Jcli3812.1

Saji, N. H., Goswami, B. N., Vinayachandran, P. N., & Yamagata, T. (1999). *Nature*, 401(6751), 360–363. https://doi.org/10.1038/43855

Schott, F. A., & McCreary, J. P. (2001). The monsoon circulation of the Indian Ocean. *Progress in Oceanography*, *51*(1), 1–123. https://doi.org/10.1016/S0079-6611(01)00083-0

Schwarzkopf, F. U., & Böning, C. W. (2011). Contribution of Pacific wind stress to multi-decadal variations in upper-ocean heat content and sea level in the tropical south Indian Ocean. *Geophysical Research Letters*, *38*, L12602. https://doi.org/10.1029/2011GL047651

Shi, G., Ribbe, J., Cai, W., & Cowan, T. (2007). Multidecadal variability in the transmission of ENSO signals to the Indian Ocean. *Geophysical Research Letters*, *34*, L09706. https://doi.org/10.1029/2007GL029528

Smith, T. M., Reynolds, R. W., Peterson, T. C., & Lawrimore, J. (2008). Improvements to NOAA's historical merged Land–Ocean surface temperature analysis (1880–2006). *Journal of Climate*, *21*(10), 2283–2296. https://doi.org/10.1175/2007jcli2100.1

Torres, M. E., Colominas, M. A., Schlotthauer, G., & Flandrin, P. (2011). A complete ensemble empirical mode decomposition with adaptive noise. Paper presented at IEEE International Conference on Acoustics, Speech and Signal Processing.

Tozuka, T., Luo, J.-J., Masson, S., & Yamagata, T. (2007). Decadal modulations of the Indian Ocean Dipole in the SINTEX-F1 coupled GCM. *Journal of Climate*, *20*(13), 2881–2894. https://doi.org/10.1175/jcli4168.1

Trenberth, K. E. (1997). The definition of El Nino. *Bulletin of the American Meteorological Society*, *78*(12), 2771–2777. https://doi.org/10.1175/1520-0477(1997)078%3C2771:tdoeno%3E2.0.co;2

Ummenhofer, C. C., Biastoch, A., & Böning, C. W. (2017). Multidecadal Indian Ocean variability linked to the Pacific and implications for preconditioning Indian Ocean Dipole events. *Journal of Climate*, *30*(5), 1739–1751. https://doi.org/10.1175/jcli-d-16-0200.1

Webster, P. J., Moore, A. M., Loschnigg, J. P., & Leben, R. R. (1999). Coupled ocean-atmosphere dynamics in the Indian Ocean during 1997-98. *Nature*, *401*(6751), 356–360. https://doi.org/10.1038/43848

Xie, P. P., & Arkin, P. A. (1997). Global precipitaion: A 17-year monthly analysis based on gauge observations, satellite estimates. *Bulletin of the American Meteorological Society*, *78*, 2539–2558. https://doi.org/10.1175/1520-0477(1997)078%3C2539:GPAYMA%3E2.0.CO;2

Yang, Y., Li, J. P., Wu, L. X., Kosaka, Y., Du, Y., Sun, C., … Feng, J. (2017). Decadal Indian Ocean dipolar variability and its relationship with the tropical Pacific. *Advances in Atmospheric Sciences*, *34*(11), 1282–1289. https://doi.org/10.1007/s00376-017-7009-2

Yang, Y., Xie, S. P., Wu, L. X., Kosaka, Y., Lau, N. C., & Vecchi, G. A. (2015). Seasonality and predictability of the Indian Ocean Dipole mode: ENSO forcing and internal variability. *Journal of Climate*, *28*(20), 8021–8036. https://doi.org/10.1175/jcli-d-15-0078.1

Yeh, S.-W. (2005). Pacific decadal variability and decadal ENSO amplitude modulation. *Geophysical Research Letters*, *32*, L05703. https://doi.org/10.1029/2004GL021731

Yu, L. S., & Rienecker, M. M. (1999). Mechanisms for the Indian Ocean warming during the 1997–98 El Niño. *Geophysical Research Letters*, *26*(6), 735–738. https://doi.org/10.1029/1999GL900072

Yuan, D. L., Zhou, H., & Zhao, X. (2013). Interannual climate variability over the tropical Pacific Ocean induced by the Indian Ocean Dipole through the Indonesian Throughflow. *Journal of Climate*, *26*(9), 2845–2861. https://doi.org/10.1175/jcli-d-12-00117.1

Yuan, Y., Chan, C. L. J., Zhou, W., & Li, C. (2008). Decadal and interannual variability of the Indian Ocean Dipole. *Advances in Atmospheric Sciences*, *25*(5), 856–866. https://doi.org/10.1007/s00376-008-0856-0